Chemical Engineering Journal 381 (2020) 122512

Contents lists available at ScienceDirect

Chemical Engineering Journal

journal homepage: www.elsevier.com/locate/cej

Hydrogen chloride removal from hydrogen gas by adsorption on hydrated ion-exchanged zeolites

Ravi Sharma[a], Tiriana Segato[b], Marie-Paule Delplancke[b], Herman Terryn[c], Gino V. Baron[a], Joeri F.M. Denayer[a], Julien Cousin-Saint-Remi[a,*]

[a] Chemical Engineering Department, Vrije Universiteit Brussel, Pleinlaan 2, B-1050, Belgium
[b] Department of Materials Engineering, Characterization, Synthesis and Recycling, Université Libre de Bruxelles, B-1050, Belgium
[c] Electrochemical and Surface Engineering Research Group, Vrije Universiteit Brussel, Pleinlaan 2, B-1050 Elsene, Brussels, Belgium

HIGHLIGHTS

- A fixed-bed method is proposed to test materials for HCl removal from hydrogen gas.
- Zeolite X was the best performing material among screened zeolites.
- Ion-exchanged X zeolites were successfully produced, characterized and evaluated.
- HCl removal from hydrogen gas occurred through reaction with the zeolite cations.
- Cation type and hydration significantly influenced the HCl removal performance.

GRAPHICAL ABSTRACT

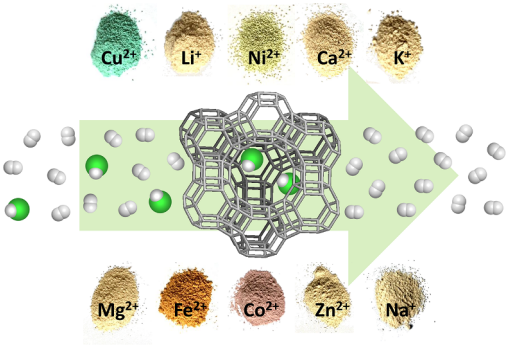

ARTICLE INFO

Keywords:
Hydrogen gas
HCl removal
Adsorption
Ion-exchanged zeolite

ABSTRACT

Hydrogen chloride is found in important hydrogen gas streams of the chemical industry and needs to be removed for safety and environmental concerns. Here, a systematic study is presented on HCl removal from hydrogen gas by adsorption on zeolites, including cation free and high cation loaded materials, as well as ion-exchanged zeolites (with alkali, alkaline earth and transition metal ions). The HCl removal performance was studied by a fixed-bed breakthrough method under high gas velocities (> 0.3 m/s), at high pressures (30 bar) and at room temperature, and with low HCl concentrations (< 200 ppm). The zeolite screening indicated that the 13X zeolite outperforms the other tested materials. The ion-exchanged X zeolites were extensively characterized via SEM-EDX, XRD, ATR-FTIR, TGA and argon adsorption isotherms. The results revealed that the ion-exchange was successfully achieved with expected tendencies in XRD and ATR-FTIR spectra, and porosities. The breakthrough experiments demonstrated that the hydration of the zeolite prior HCl adsorption improves the hydrogen gas purification performance. The characterization after HCl adsorption supports the hypothesis that HCl is taken up by the material by forming salt molecules within the zeolite cavities by reaction with the cations and, which is, moreover, enhanced by the presence of pre-adsorbed water. The type of cation present in the zeolite framework structure notably affected the HCl removal adsorption capacity as well as uptake rate. Among the ion-exchanged zeolite samples, the Zn^{2+} form exhibited the highest adsorption capacity at saturation, attributed to the over-exchange of the zeolite cations. The investigation revealed important parameters such as cation radius, atomic mass and electronegativity, which played a noteworthy role in defining the HCl removal performance of ion-exchanged zeolites.

* Corresponding author.
E-mail address: jcousins@vub.be (J. Cousin-Saint-Remi).

https://doi.org/10.1016/j.cej.2019.122512
Received 9 April 2019; Received in revised form 10 August 2019; Accepted 14 August 2019
Available online 14 August 2019

1. Introduction

Hydrogen gas is the cleanest fuel [1–3] and finds widespread applications in our society: from oil refining [4,5] and metal welding [6] to the production of ammonia [4], semiconductors [4,6] and pharmaceuticals [7]. With its numerous advantages compared to traditional fuels, including a higher energy content, no pollution during combustion and its ability to be stored in any form (i.e. gas, liquid or solid), hydrogen gas is expected to shape the future global energy markets [8,9]. Hydrogen, though not readily available in nature, can be produced from varieties of feedstocks which include fossil and renewable resources [8,9]. Nowadays, hydrogen gas is mainly produced as a by-product of the chemical industry obtained during the reforming of hydrocarbons [2,9]. During this process the catalyst is typically promoted with chlorine to enhance the process performance [10–12], however, this also comes along with the formation hydrogen chloride (HCl) impurities in the product streams. Besides the contamination of the product stream, HCl may cause severe corrosion, fouling and equipment damage, leading to potentially serious safety and environmental issues [10–14]. Therefore, removal of hydrogen chloride from hydrogen gas is of great importance for chemical industry and the environment.

Among the different techniques used to purify hydrogen gas, such as partial condensation [15], chemical reactions [16], membrane and molecular sieve separations [15,16], the preferred approach used in the chemical industry is absorption at high temperatures on mineral based absorbents [17–29]. Adsorption at low temperatures, offers a very selective and energy-efficient alternative [30,31], however, it is particularly challenging to achieve an efficient HCl removal at high gas velocities and low concentrations. Although the adsorption of impurities such as hydrogen sulfide, carbon monoxide and ammonia have been studied on various adsorbents, including hydroxide and carbonate based adsorbents [32–35], active carbon [36–38], zeolites [34,39,40] and MOFs [31], the adsorptive removal of HCl from hydrogen gas at low temperatures remains almost unexplored, and in particular for zeolites [41,42]. Kim et al. carried out HCl adsorption and desorption breakthrough experiments with 13X pellets packed beds at high pressure and gas velocities under nitrogen environment [43]. Micoli et al. evaluated the HCl removal performance of Cu and Zn exchanged and impregnated 13X zeolite materials from nitrogen at low pressures for biogas purification [14].

Ion-exchange is known for decades to allow a fine control of the (equilibrium and kinetic) adsorption and catalytic properties of zeolites [44–47]. More recently, for example, Baksh et al. [48] showed that the N_2/O_2 adsorption selectivity was significantly improved by replacing the Na^+ cation by Li^+ in the X zeolite material. Such improvement was also observed for capturing CO_2 using ion-exchanged zeolite beta (BEA) [49]. Walton et al. [50] performed a systematic study on CO_2 adsorption using ion-exchanged Y and X, demonstrating clear differences in adsorption capacities attributed to the zeolite cations. Another study indicated that the permeance and selectivity of zeolite membranes for the CO_2/N_2 separation could be tuned by playing with the exchangeable cations [51]. Bonenfant et al. [52] suggested that the CO_2 adsorption is principally governed by the cations that induce basicity and an electric field in the zeolite cavities. Furthermore, the removal of toxic metals such as lead and cadmium from waste water was also explored with (natural) zeolites treated with electrolyte solutions [53]. On the other hand, apart from adsorptive separations, ion-exchanged zeolites have been proven quite useful in catalytic reactions, such as decomposition of NO with the Cu-MFI (over-exchanged) zeolite material [54]. Yet, to our best knowledge no systematic study on the HCl removal performance of ion-exchanged zeolites has been conducted so far.

Therefore, a systematic study is presented here on the removal of HCl from hydrogen gas by adsorption on zeolites, including cation-free and ion-exchanged materials. Ion-exchanged zeolite materials are produced containing alkali, alkaline and transition metal cations. The HCl removal performances are explored via breakthrough experiments under dynamic (process) conditions. The adsorbents are extensively characterized via X-rays diffraction (XRD), scanning electron microscopy (SEM) coupled with energy dispersive X-ray spectroscopy (EDS), attenuated total reflectance infrared spectroscopy (ATR-FTIR) and argon porosimetry, as well as thermogravimetric analysis (TGA). The HCl adsorption mechanism is unraveled, including the effects of cation and material properties.

2. Experimental

2.1. Adsorbents and chemicals

The zeolites used in this study are listed in the Table 1 with their properties as specified by the suppliers. The 13X and A zeolites were in pellet or bead form containing a binder, while the silicalite was a binder-free powder (Table 1). Prior to any further treatment, the materials were shaped into pellets with a particle size ranging from 200 to 280 μm (Fig. 1). For all materials except silicalite, this was achieved by crushing the materials followed by a sieving step. The effect of crushing on the adsorption properties of the native material was confirmed to be negligible (Fig. S1). For silicalite, the pellets were made by compacting powder into a cake with a hydraulic French press (Piqua, USA) at a pressure of 65 MPa, which was subsequently broken and sieved.

Ion-exchange solutions were made of Millipore water and different metal salts: zinc nitrate hexahydrate ($Zn(NO_3)_2.6H_2O$, 99%, Fluka Chemika), copper nitrate trihydrate ($Cu(NO_3)_2.3H_2O$, 99%, Sigma Aldrich), iron sulphate heptahydrate ($FeSO_4.7H_2O$, 99%, Sigma Aldrich), cobalt chloride hexahydrate ($CoCl_2.6H_2O$, 98%, Acros), nickel nitrate hexahydrate ($Ni(NO_3)_2.6H_2O$, 98%, Merck), lithium chloride (LiCl, 99%, Sigma Aldrich), magnesium chloride hexahydrate ($MgCl_2.6H_2O$, 99%, Sigma Aldrich), calcium chloride hexahydrate ($CaCl_2.6H_2O$, 99%, Sigma Aldrich) and potassium chloride (KCl, 99%, Riedel-de Haën).

Gas streams used in the breakthrough experimentation (see further) were composed of pure hydrogen gas (Premium Plus X50S, Air Products) and hydrogen gas containing hydrogen chloride (1.008 mole % ± 0.5% relative, Air Products). The hydrogen chloride content was verified by gas absorption in a water column and a pH meter (InoLab, pH 7110, WTW).

2.2. Zeolite modification via ion exchange

The ion-exchange was performed by treating 0.5 g of 13X pellets (*vide supra*) with 50 mL of 0.5 M metal salt solution (see above) under stirring at room temperature for 50 h. The pH of the electrolyte solutions was determined with a calibrated pH meter (InoLab, pH 7110, WTW). In addition, the ion-exchange solution was renewed every 10 h. Afterwards, the solid was separated from the liquid and washed with deionized water (250 ml and 3 times). Finally, the treated pellets were dried at 80 °C overnight. The reproducibility of the ion-exchange method was confirmed via chemical analysis and HCl breakthrough experiments (see Supporting Information, Section S2).

Table 1
Zeolites with their properties as specified the suppliers.

Name	Appearance	Supplier	Framework	Si/Al	Cation
5A	Beads	CECA	LTA	1.0	Ca^{2+}
4A	Beads	CECA	LTA	1.0	Na^+
3A	Beads	CECA	LTA	1.0	K^+
13X	Pellets	UOP Molsiv	FAU	1.23	Na^+
Silicalite	Powder	Alsi-Penta	MFI	> 500	Na^+

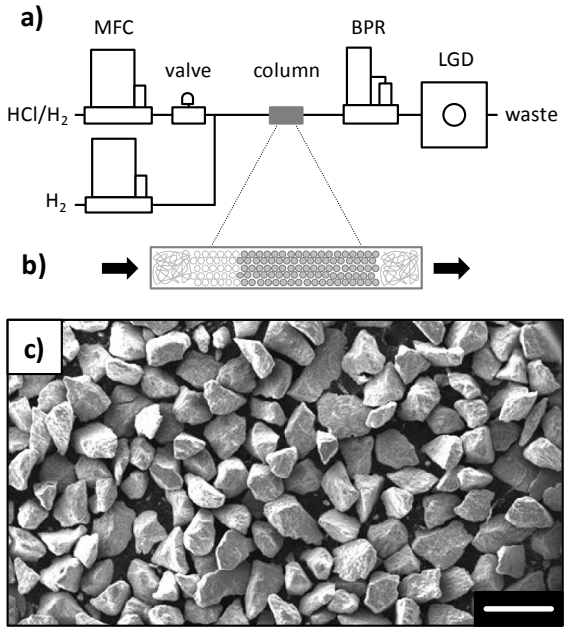

Fig. 1. a) Scheme of HCl breakthrough setup with mass flow controllers (MFC), backpressure regulator (BPR) and on-line laser gas detector (LGD). b) Packed column filled with quartz wool, quartz beads (light) and zeolite pellets (dark). c) SEM image of pellets from the native X material (scale bar: 500 µm).

2.3. Breakthrough experimentation

Gas phase breakthrough experiments were carried out with packed columns placed in an in-house made setup (Fig. 1). Columns (i.e. 3.9 cm length and 0.22 cm inside diameter) were packed with 100 mg of pellets surrounded by quartz beads and wool (Fig. 1) under ambient conditions. Experiments were performed at room temperature (294 K) and at a total pressure of 30 bar.

First, the setup was saturated with the selected HCl/H_2 mixture without column. Afterwards, following a quick flush of the setup with pure hydrogen gas, the empty column was replaced by the packed column. Finally, the material was contacted with HCl by changing the feed from pure hydrogen gas to a hydrogen gas stream containing 200 ppm HCl. The gas composition was controlled by calibrated mass flow controllers, mixing a pure hydrogen gas and hydrogen gas containing HCl (see above). The gas velocity was set at 0.34 m/s. HCl was detected at the column outlet with an on-line calibrated laser detector (Axetris, Switzerland). Breakthrough curves were obtained by plotting the HCl concentration, detected at the column outlet, in function of time. The amount HCl adsorbed q (*g*/*g*) was calculated from the mass balance over the column, using Eq. (1):

$$q = \frac{(F\tau - \varepsilon V)}{m_{ads}} \frac{yp}{RT} M \quad (1)$$

with F, τ, ε, V, m_{ads}, y, p, R, T and M representing the (volumetric) feed flow rate (ml/min), the average breakthrough time (min), the bed porosity, the column volume (ml), the mass adsorbent (g), the HCl volume fraction in the feed, the total pressure (bar), the gas constant (J/K/mol), the temperature (K) and the HCl molar mass (g/mol). The feed volumetric flow rate (and gas velocity) was calculated from the column dimensions, the pressure in the column and the volumetric flow rate at the setup outlet. The latter was measured with a bubble flow meter. The average breakthrough time was calculated from Eq. (2):

$$\tau = \int_0^\infty \left(1 - \frac{c}{c_o}\right) dt \quad (2)$$

with c and c_o denoting the HCl concentration at the column outlet and the feed concentration, respectively. The reproducibility of the experimental approach is presented in the Supporting Information (Section S3). In addition, the adsorption capacity at 1 ppm breakthrough is determined by integration of Eq. (2) until 1 ppm is detected at the column outlet.

Dried samples were obtained by heating the pellets, prior packing them into the columns, into an oven from 298 to 363 K at 1 K/min, followed by an increase to 623 K at 0.5 K/min. The samples were then kept at 623 K during 12 h. Afterwards, the samples were cooled down and packed in a column inside a nitrogen glove-box. The column was then transferred to the HCl breakthrough setup with both ends sealed. A water saturated sample was obtained at room temperature by sending a water enriched vapor stream through a packed column containing (untreated) pellets that were previously packed under ambient conditions. The water enriched vapor stream was generated by bubbling pure helium (He) through a vessel filled with pure liquid water (Millipore) at a flow rate of 20 Nml/min and a water partial pressure of 27.6 mbar.

A cyclic adsorption-desorption HCl breakthrough experiment was performed by changing the feed to pure hydrogen gas after saturation of the column with HCl (see above for details about the conditions). The desorption was carried out with a pure hydrogen gas stream which was sent to the column at a flow rate of 2 Nl/min and a total pressure of 1.85 bar during 17 hours. Afterwards, the HCl breakthrough experiment (in adsorption mode) was repeated by changing back to the HCl/H_2 gas mixture under the same conditions as the first adsorption step (*vide supra*).

Table 2
Structural and chemical properties of cations and ion-exchanged X zeolites.

Cation	Alkali			Alkaline		Transition				
	Na^+	Li^+	K^+	Ca^{2+}	Mg^{2+}	Fe^{2+}	Co^{2+}	Ni^{2+}	Cu^{2+}	Zn^{2+}
radius (Å) [70]	0.99	0.60	1.37	1.03	0.72	0.75	0.72	0.71	0.72	0.74
hydrated radius (Å) [70]	3.58	3.82	3.31	4.12	4.28	4.28	4.23	4.04	4.19	4.30
electronegativity [71]	0.93	0.98	0.82	1.00	1.31	1.83	1.88	1.91	1.90	1.65
atomic mass	23.0	6.9	39.1	40.1	24.3	55.8	58.9	58.7	63.6	65.4
anion	Cl^-	Cl^-	Cl^-	Cl^-	Cl^-	SO_4^{2-}	Cl^-	NO_3^-	NO_3^-	NO_3^-
charge exchange (%)[a]	100	83	94	87	72	96	80	81	100	80
Si/Al ratio[a]	1.42	1.39	1.44	1.44	1.40	1.88	1.34	1.40	1.49	1.38
M/Al charge ratio[a]	0.97	1.00	1.07	0.86	1.07	1.58	1.09	1.18	2.37	1.75
crystallinity (%)[b]	80	80	76	77	81	27	80	78	54	83
micropore vol. (cc/g)[c]	0.18	0.18	0.18	0.24	0.23	0.01	0.21	0.17	0.02	0.20
total pore vol. (cc/g)[c]	0.32	0.34	0.30	0.42	0.37	0.14	0.35	0.30	0.19	0.35

[a] Determined via EDX analysis.
[b] Obtained from XRD measurements.
[c] Calculated from argon isotherm.

2.4. Gravimetric method

The vapor phase adsorption isotherm of water was measured with a gravimetric technique (VTI, USA). About 5 mg of zeolite pellets were place in a sample holder and activated under a pure nitrogen flow (180 NmL/min) during 5 h at 623 K (1 K/min increase from 298 K). After cooling the sample to 323 K, the feed was switched from pure nitrogen to an enriched water vapor stream. The sample weight was followed until equilibrium was reached with the surrounding atmosphere. This was repeated for several different relative humidities.

2.5. Characterization techniques

The bulk textural and chemical (composition) properties were investigated via scanning electron microscopy (SEM) coupled with energy dispersive X-rays spectroscopy (EDX) using a JSM-IT300 JEOL device under vacuum (circa. 10^{-6} Torr) at a voltage of 20 kV. Zeolite particles were stabilized with carbon tape on a sample holder and coated with a carbon layer (15 nm). The Li^+ content, which could not be directly measured by EDX, was estimated from the expected charge neutrality and Si/Al ratio of the X zeolite framework structure. The atomic percentages detected by EDX analysis in the zeolite materials were used to calculate the different ratios given in Table 2 (see further). Following repeated measurements, the average deviation for the EDX analysis is estimated at 6% and maximum 11% in relative standard deviation within a same sample.

The crystallinity of the different samples was explored via X-rays diffraction (XRD) under ambient conditions. A Bruker device (D8 Advance Eco diffractometer) was used with Cu Kα radiation (40 kV, 25 mA) and a LynxEye XE-T (PSD opening 3.3°) detector in the range of 5–70° 2theta (with 0.015° step size and time 0.5 s/step).

The attenuated total reflectance – Fourier transform infrared (ATR-FTIR) spectra were recorded using a Bruker Vertex 70 V device over a frequency range of 50 – 4000 cm^{-1}. Samples were mounted under ambient conditions and analyzed under vacuum (i.e. less than 1 hPa).

Argon adsorption isotherms were measured with an Autosorb AS-1 (Quantachrome Instruments, USA). About 20 mg of material was activated by gradually heating at a rate of 2 K/min from room temperature to 623 K and kept during about 3 hours. After cooling down, adsorption isotherms were measured at 87 K and analyzed via the Gurvich rule and non-local density function theory (NLDFT) [55,56]. Porosities obtained by both approaches are compared in Table S3 (Supporting Information).

The material behavior upon heating was analyzed by thermogravimetric analysis (TGA) with a SENSYS Evo instrument (SETARAM Instrumentation). About 10 mg of material was placed in the sample holder and subjected to a gradual increase in temperature (0.1 K/min) from 303 K to 723 K under a pure helium stream (100 Nml/min). A measurement was also conducted at a constant temperature of 303 K. The sample weight was recorded in function of time.

3. Results and discussion

In this work, first an adsorbent screening is performed to select the most efficient zeolite material for HCl removal from hydrogen gas. Subsequently, the selected material is ion-exchanged and characterized in depth. Afterwards, the HCl adsorption mechanism and removal performances as a function of exchanged cation are studied.

3.1. Adsorbent screening

The hydrogen chloride (HCl) removal performance (from hydrogen gas) of various zeolites i.e. 13X, silicalite, 3A, 4A and 5A was evaluated via breakthrough experimentation with packed beds. Fig. 2 shows the HCl breakthrough profiles (Fig. 2a) and the corresponding HCl adsorption capacities obtained at saturation and at 1 ppm (Fig. 2b). It clearly demonstrates that the 13X zeolite outperforms all other zeolites investigated in this study. For instance, the average breakthrough time and adsorption capacities are at least a factor six larger for 13X compared to the other zeolites. In addition, since the 13X zeolite also exhibits a sharp HCl elution profile (Fig. 2a), its adsorption capacity at 1 ppm does not deviate substantially from that obtained at saturation. This is of particular importance, because the purification performance of a fixed-bed adsorber is determined at initial breakthrough [57].

The large difference in HCl adsorption capacity between 13X and the other zeolites can be explained by a steric effect, but also due to the presence of extra-framework cations. The 3A, 4A and 5A zeolites exhibit pore entrances with a diameter of 3.3 Å [58], 4.2 [59] Å, and 5.0 Å respectively [60], whereas 13X possesses a large pore opening of 7.4 Å [61]. Considering the kinetic diameter of HCl, being 4.42 Å [62], HCl may thus be excluded from zeolite A cavities, in particular if being hydrated (see further for additional discussion), while being readily able to enter the 13X pores. Although silicalite features a larger pore diameter (i.e. 5.7 Å [63]), than the A zeolites, it has (almost) no extra-framework cations. Therefore, the low HCl adsorption capacity of silicalite could originate from this absence of cations which may serve as adsorption sites for HCl [64,65], however, it may also have been a contribution of differences in zeolite basicity [64]. The investigation of the differences in HCl adsorption mechanism between the screened materials lays beyond the scope of this work. Following the adsorbent screening, the best performing material, namely the 13X zeolite, was selected to be ion-exchanged and further evaluated for HCl removal from hydrogen gas by adsorption.

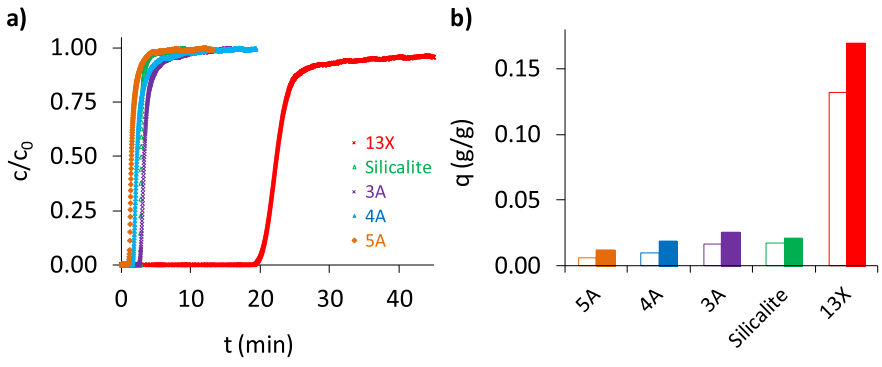

Fig. 2. HCl removal performances of different zeolites at 298 K, 6.39 mbar HCl partial pressure, 0.34 m/s gas velocity and 30 bar total pressure. a) HCl breakthrough profiles and b) HCl adsorption capacities obtained at saturation (filled) and at 1 ppm (empty).

3.2. Ion-exchanged X zeolites

The 13X zeolite extraframework cation (i.e. Na^+) was exchanged for different alkali (Li^+ or K^+), alkaline (Ca^{2+} or Mg^{2+}) or transition metals (Fe^{2+}, Co^{2+}, Ni^{2+}, Cu^{2+} and Zn^{2+}) using various electrolyte solutions. The resulting materials were characterized by various methods, as explained below (Figs. 3–5 and Table 2). First, SEM images (Fig. S4) indicate that the bulk structure of the pellets and primary particles (i.e. the zeolite crystals) is well preserved for most samples after the ion-exchange treatment. Only for the Fe^{2+} and Cu^{2+} forms, clear differences are observed with the native material (Na^+ form) (Fig. S5). The Cu^{2+} form displays new small crystals on the pellet surface that are different from the primary particles found in the native material. These new crystals are most likely Cu^{2+} salt deposits. For the Fe^{2+} form, the SEM images clearly evidence a dramatic change in pellet structure (Fig. S5). The Fe^{2+} ion-exchange treatment has generated a honeycomb type structure where the primary particles of the native material disappeared almost completely (Fig. S5). These observations suggest that the native material is significantly affected or degraded after being contacted with the Cu^{2+} and Fe^{2+} electrolyte solutions.

Next, EDX analysis reveals the presence of the desired cation (Fig. S6), but also that the native cation (i.e. Na^+) remains in all samples, except for the Cu^{2+} sample. The amount of desired cation, given in Table 2, shows that the ion-exchange was successfully achieved, however, except for copper, iron and potassium, its extent for all other cations was limited to about 80%. This may originate from the inability of hydrated cations to enter the sodalite cages of the structure. Most hydrated cations possess much larger radii than the sodalite cage entrance (i.e. 2.53 Å [61]). Therefore, the Na^+ cations will (partly) remain in the material, leading to incomplete ion exchange [65–67]. In addition, EDX analysis also indicates that, with the exception for Fe^{2+}, the Si/Al ratio remains almost constant after the ion-exchange treatment of the native material (Na^+ form) with the different electrolyte solutions. Also, it is interesting to note that certain samples are over-exchanged (Fe^{2+}, Cu^{2+} and Zn^{2+}), as seen from the charge ratio (Table 2). More cations are present in these samples than necessary to achieve charge neutrality in the zeolite structure. Since the ion-exchange, based on the charge, is not 100%, other metal species, than the cationic form, may have been taken up during the contact with the electrolyte solutions. Over-exchanged zeolites were also produced in earlier studies [54,68,69] and it was proposed that the cation over-exchange originates from the uptake of metal hydroxides and clusters during the ion-exchange from aqueous solutions [68].

The X-rays diffractograms, shown in Fig. 3, demonstrate that most samples, except for the Fe^{2+} and Cu^{2+} forms, maintain the crystalline structure of the native material after ion-exchange, with all major peaks matching with those reported for the FAU structure of the X zeolite [72]. Smaller peaks around 12, 17, 25 and 28° are differently located for the different samples. This could be explained by differences in cation relocation [73] and framework distortion [74]. In addition, about 20% amorphous fraction is detected for most samples, which is attributed to the presence of a binder in the native material (Table 2). On the other hand, the substantial decline in crystallinity was observed in the cases of Fe^{2+} and Cu^{2+}. This can be explained by the acidic nature of their respective aqueous solutions. For instance, all electrolyte solutions had a pH around 5.5, however, those of Fe^{2+} and Cu^{2+} were 3.6 and 3.5 respectively. Such acidic environment may lead to the deterioration of the zeolite framework structure and thus, a lower crystallinity [75]. Similar findings were mentioned by Holmberg et al. [76]. They observed that at a pH 3, the FAU structure of zeolite Y begins to break down.

ATR-FTIR spectra, shown in Fig. 4, illustrate the same tendencies as observed by XRD after ion-exchange. While most samples possess very similar spectra (Figs. 4 and S11), with major peaks originating from Si-O-Al vibrations in the zeolite framework structure [77], the Cu^{2+} and Fe^{2+} forms exhibit broader profiles with more pronounced OH-stretching vibrations peaks ($> 3000\ cm^{-1}$). The treatment of the native adsorbent material with the Cu^{2+} and Fe^{2+} electrolyte solutions for ion-exchange may have degraded the zeolite framework structure, which was also pointed out by the XRD (Fig. 3). Besides that, the IR spectra show an interesting tendency between the various samples. The single charged cation samples display a single peak around $964\ cm^{-1}$, while two peaks are observed for double charge cation samples. Except for Cu^{2+} and Fe^{2+} forms, these differences are attributed to the exchanged cations in the zeolite framework structure [78].

Fig. 5 displays the argon (adsorption) isotherms of the different samples. First, the argon adsorption isotherm of the native X material (i.e. the Na^+ form) has lower capacities compared to other data reported in the literature [79]. Since a formulated 13X is used in this study, it is expected that the adsorption capacities are lower than for a pure (unformulated) 13X sample due to the presence of a binder. However, the difference appears larger than simply the amount of binder present in the native material (i.e. about 20%, estimated as the amorphous fraction determined by XRD). Differences in adsorption capacities between various commercial samples are seen in the literature [80]. Pore-blocking by the binder may explain the lower than expected adsorption capacities for this simple [81]. On the other hand, since the shape of the argon adsorption isotherm (Fig. 5), the crystallinity (Fig. 3), as well as the infrared bands (Fig. 4) and the Si/Al ratio (Table 2) remain almost constant for most samples, the results are expected to be solely an expression of the ion-exchange in the zeolite crystals rather than the modification of the binder fraction by the different electrolyte solutions. Second, although most samples possess similar argon isotherms, the Fe^{2+} and Cu^{2+} materials clearly exhibit much lower capacities. This is consistent with the XRD and ATR-FTIR observations (Fig. 3,4) which indicated that the crystalline structure of these materials was (partly) destroyed after ion-exchange (Fig. 3 and Table 2), leading to smaller (relative) micro- and total porosities (Fig. 5 and Table 2). On the other hand, the samples which retained a high crystallinity also conserved similar porosities as the native material (Table 2). However, some interesting differences can still be noticed between these samples. For instance, while for the alkali metal ion samples (Li^+ and K^+) no significant change was observed in micro- and total pore volume, the alkaline metal ion materials (Ca^{2+} and Mg^{2+}) clearly exhibit larger pore volumes than the native material (i.e. Na^+ form) (Table 2). A similar effect was also noticeable for the transition metal ion forms of Co^{2+} and Zn^{2+}, but not for Ni^{2+} (Table 2). The increase in the micropore volume, detected for the Ca^{2+}, Mg^{2+}, Co^{2+} and Zn^{2+} forms (Table 2), results from the opening of the pores by an exchange of 2 mol of single charged cations for 1 mol of double charged cations in the FAU structure of the X zeolite [57]. In case of the Ni^{2+} form, despite having equivalent radii as the other doubled charged cations (Table 2), no significant variation in porosity was noticed

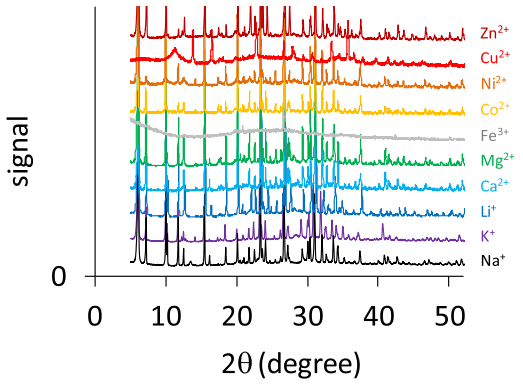

Fig. 3. XRD patterns of ion-exchanged X zeolites, with the native material being the Na^+ form (13X).

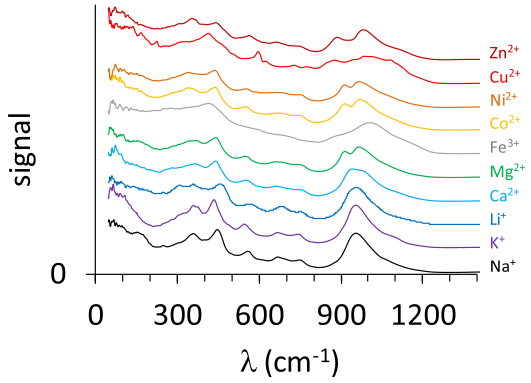

Fig. 4. ATR-FTIR spectra of ion-exchanged X zeolites, with the native material being the Na^+ form (13X).

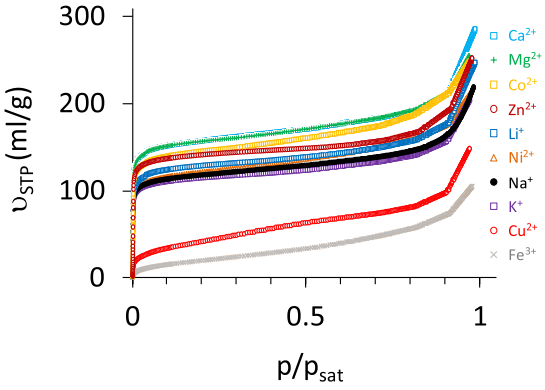

Fig. 5. Argon adsorption isotherms of ion-exchanged X zeolites, with the native material being the Na^+ form (13X).

compared to the native X material (Na^+ form). Previous studies on ion-exchange Y zeolites (FAU topology) also reported similar results for the Ni^{2+} form [82,83]. It was suggested that some cations may lead to pore-blocking [83], which reduces the material porosity. Following the above-made observations the Fe^{2+} and Cu^{2+} forms were excluded for further examination in this study.

3.3. HCL removal performance

3.3.1. Effect of zeolite hydration

First, the effect of zeolite hydration on the HCl removal performance is studied on the native (13X) material. Fig. 6 shows the water vapor phase adsorption isotherm obtained by the gravimetric method (Fig. 6a), the (water) desorption curve measured by TGA (Fig. 6a) and, the results from HCl breakthrough experiments with dried and hydrated materials (Fig. 6c,d) (see Material and Methods Section for more detail). As expected from the literature, water shows a steep Type I isotherm shape (Fig. 6a) [84–86], indicating the high affinity for the X zeolite material. Under ambient conditions (RH > 30%), the material is, thus, considered to be (almost) fully saturated with water vapor. The amount adsorbed at saturation agrees well with the micropore volume determined by argon porosimetry (Table 2). The adsorption capacities are, however, lower than for other commercial samples [87,88]. The origin of this was attributed to the presence of the binder (*vide supra*). Next, the desorption curve indicates that the material is only completely dehydrated by heating at temperatures above 300 °C (Fig. 6b). This is consistent with the literature, and almost identical behaviors were observed for different ion-exchanged X zeolites [89–91]. The stepped shape of the desorption curve may be assigned to the different adsorption sites in the zeolite structure [92]. On the other hand, without heating, a pure inert gas flow (at constant temperature of 303 K) appears to only remove a limited amount of water from the material pores (Fig. 6b). Therefore, under hydrogen gas, which may be considered inert with its negligible adsorption capacities on zeolites [93], and the short (fluid) contact time (i.e. 0.11 s), the ion-exchanged

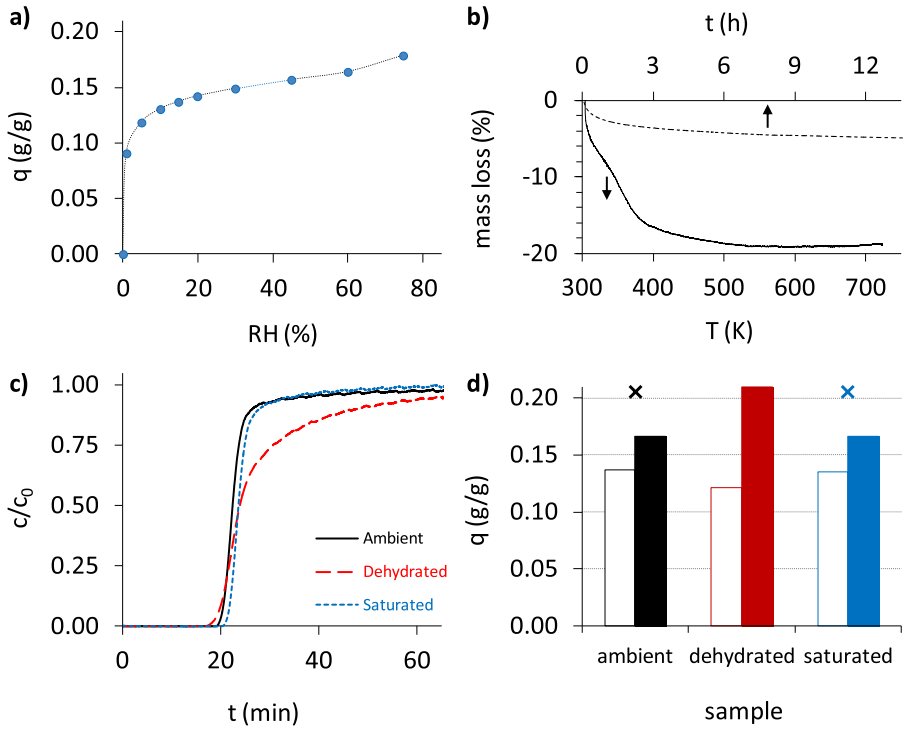

Fig. 6. a) Vapor phase adsorption isotherm of water on the native material at 323 K. b) Desorption curves with temperature program (full) and at 303 K (dashed). c) HCl breakthrough profiles of dried and hydrated materials, measured at 298 K, 6.39 mbar HCl partial pressure, 0.34 m/s gas velocity and 30 bar total pressure. d) HCl adsorption capacities determined from breakthrough curves in Fig. 6c at saturation (filled) and at 1 ppm (empty), and at saturation per dry mass material (cross).

materials are expected to remain hydrated during the breakthrough experimentation until the contact with HCl occurs.

Following these observations, the HCl removal performance of the native material was studied for three pre-treatments: loaded under ambient conditions, dried at 623 K and saturated with water vapor (see Material and Methods Section for more detail). Fig. 6c presents the HCl breakthrough profiles for the different cases. The corresponding adsorption capacities are shown in Fig. 6d. The breakthrough profiles (Fig. 6c) indicate that the material previously saturated with water takes up HCl in almost an identical fashion as the material being loaded under ambient conditions. This is in line with the water adsorption isotherm (Fig. 6a) showing that under ambient conditions the material is almost completely saturated with water. The small difference in loading will not significantly affect the HCl uptake by the zeolite material (Fig. 6c,d). On the other hand, the dried sample behaves very differently than the other two samples (i.e. ambient and saturated). While sharp HCl profiles are observed for the ambient loaded and water saturated samples, the dehydrated material displays an earlier HCl breakthrough and a much broader profile. As a result, the dehydrated material possesses a much lower adsorption capacity at a breakthrough point of 1 ppm, than at saturation (Fig. 6d). The broadening of the elution profile results from mass transfer resistances or limitations in reaction kinetics [53], indicating that these are more pronounced with the dehydrated sample than for the hydrated samples. This may originate from the difference in cation location within the X zeolite framework structure between the hydrated and dehydrated state [94] and/or the absence of water which may promote the HCl (reactive) uptake, rather than a degradation of the material structure due to the activation. XRD reveals that the dried material after contact with HCl preserved the (crystalline) characteristics of the native material (Fig. S8). On the other hand, the dried material adsorbs more HCl than the hydrated samples per mass loaded material (Fig. 6d). However, by taking in account the degree of dehydration at 623 K measured by TGA (Fig. 6b), almost identical adsorption capacities are retrieved per mass dried material. In conclusion, since the drying of the adsorbent resulted in unfavorable fixed-bed dynamics with a lower adsorption capacity at 1 ppm breakthrough point than hydrated samples, the HCl removal performance of ion-exchanged X zeolites was further studied with (ambient) hydrated samples.

3.3.2. HCL adsorption mechanism

In order to gain insight into the nature and mechanism of HCl adsorption on the X zeolite adsorbent, the properties of the native material were compared before and after HCl contact (Fig. 7). The adsorption properties were explored by a cyclic breakthrough experiment (Fig. 7a), while the chemical and structural properties were studied via EDX (Fig. 7b), XRD (Fig. 7c) and ATR-FTIR (Fig. 7d) analyses. In addition, the thermal behavior was studied by thermogravimetric analysis (Fig. S9). Fig. 7a shows the elution profiles of HCl from a (continuous) cyclic breakthrough experiment, including the HCl breakthrough profile measured on the column (A1), the desorption from it with pure hydrogen gas (D1) and followed by a second adsorption step (A2).

The immediate breakthrough of HCl (in Fig. 7a, A2), from the packed column which was previously saturated with HCl (A1) and subsequently flushed with pure hydrogen gas (D1), indicates that no adsorption capacity is retrieved after purging the adsorber overnight at a high volumetric flow rate. In addition, no significant difference in adsorption capacity is observed between 0.04 and 6.39 mbar HCl partial pressures (Fig. S10). Together with the desorption behavior (Fig. 7a, D1), it proves that the adsorption isotherm has a rectangular shape, resulting in sharp breakthrough profiles with a significant breakthrough time (Fig. 7a, A1) and very difficult desorption of HCl (Fig. 7a, D1) [57]. The bumps, observed in the second adsorption step of the cyclic breakthrough experiment (Fig. 7a, A2), are attributed to the valve and back pressure regulator as also seen from a blank measurement (Fig. S3). These adsorption dynamics demonstrate that HCl has a very high affinity for the X zeolite material. This is also evidenced by the EDX analysis and the behavior upon heating studied by thermogravimetric analysis. For instance, the EDX spectra clearly reveal the presence of chlorine in the material (at 2.6 keV, Fig. 7b) even under high vacuum and the use of an electron beam used during the analysis. The TGA curve measured after HCl contact (Fig. S9) indicates that the

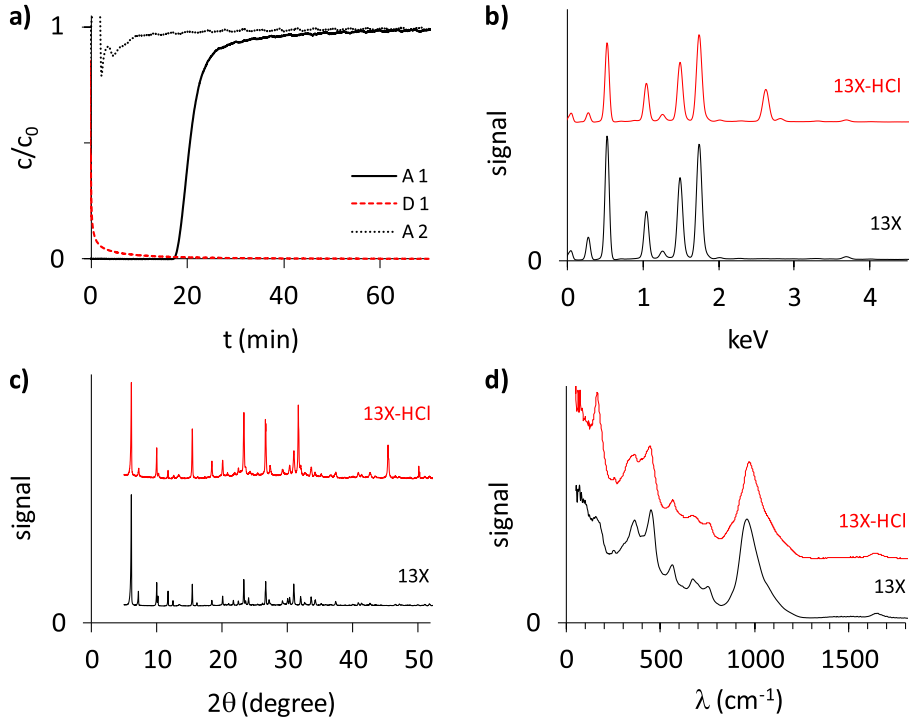

Fig. 7. a) HCl elution profiles of a (continuous) cyclic experiment with (A1) the first adsorption step, (D1) the desorption step between both adsorption steps and (A2) the second adsorption step. b) EDX spectra, c) XRD patterns and d) ATR-FTIR spectra of X zeolite material before and after HCl contact.

material losses mass only at much higher temperatures compared to the (ambient) water saturated sample (Fig. 7b). Since (almost) no adsorption was observed with a cation-free material with accessible (large) pores, the high affinity is attributed to the presence of the cations in the framework structure (*vide supra*, Fig. 2). Interestingly, the adsorption capacities (Fig. 7d) indicate that for each Na^+ cation in the zeolite material about one HCl molecule is adsorbed (see Supporting Information Section 10, and also further Fig. 9). This is also confirmed by EDX analysis, however, the Cl/Na ratio is lower than the one determined from the breakthrough curve (Fig. S7). The high energy electron beam used in the EDX analysis may degrade the material under investigation and remove adsorbed molecules, as seen by the continuous decrease in Cl/Na ratio with repeating measurements (Fig. S7). On the other hand, X-rays diffraction reveals that NaCl is formed inside the zeolite pores, with new strong peaks showing up at about 31.6, 45.4 and 56.4° after HCl contact compared to the fresh material (Fig. 7c) [95,96]. In addition, the material crystallinity decreased, with the amorphous fraction increasing from 20.3% to 30.0%. Thus, the formation of NaCl comes along with the degradation of the zeolite structure. This may originate from the framework structure being unstable without cations present to neutralize the negative charge in the zeolite structure [95,97] and/or the acidic nature of the hydrogen chloride in the presence of (pre-adsorbed) water. The crystallinity might also be influenced by the presence of the adsorbed phase [95]. The formation of NaCl is also corroborated by the ATR-FTIR measurements (Fig. 7d). A strong peak is detected around 160 cm^{-1} in the infrared spectra of the zeolite material after HCl contact. This peak lies in the region of cation vibrations (i.e. $<$ 200 cm^{-1}) [98] and strong absorbance for NaCl (Fig. S12), indicating a significant change in cation properties. In conclusion, the above-discussed results support the hypothesis that the uptake of HCl from hydrogen gas by the X zeolite proceeds via chemisorption through reaction with the cations, present in the zeolite framework structure, into NaCl:

$$NaX(s) + HCl(g) \overset{H_2O(a)}{\rightarrow} HX(s) + NaCl(a) \quad (3)$$

with the pre-adsorbed water promoting the reaction by producing chlorine ions, from the adsorbed HCl, necessary for NaCl formation:

$$H_2O(a) + HCl(a) \rightleftarrows H_3O^+(a) + Cl^-(a) \quad (4a)$$

$$NaX(s) + Cl^-(a) \rightleftarrows X^-(s) + NaCl(a) \quad (4b)$$

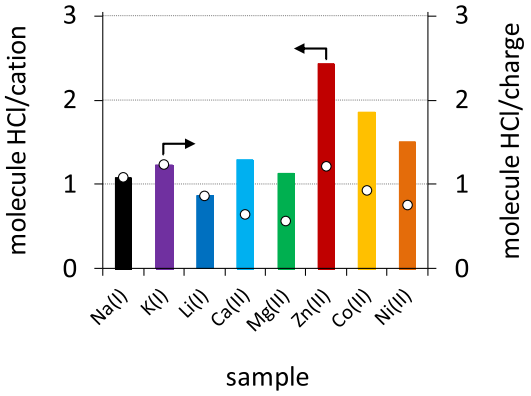

Fig. 9. HCl adsorption capacities of ion-exchanged X zeolites in terms of amount adsorbed molecules HCl per cation (left vertical axis) and per charge (right vertical axis). The values were calculated from the results shown in Fig. 8 following the procedure given in Supporting Information Section S10.

$$X^-(s) + H_3O^+(a) \rightleftarrows HX(s) + H_2O(a) \quad (4c)$$

The formation of H_3O^+ ions from co-adsorbed water and hydrogen halides was also previously observed on various hydrated systems [99]. On the other hand, without water the zeolite pore environment induces the HCl dissociation via Lewis acid-base interaction with the cation [97], however, the reaction kinetics are much less favorable than in the presence of water, as suggested by the broad HCl elution profile for the dried zeolite material (Fig. 6c).

3.3.3. Effect of cation type

The HCl removal performances of the (hydrated) ion-exchanged X zeolites were evaluated via breakthrough experiments. The breakthrough curves and corresponding adsorption capacities at saturation and 1 ppm are provided in Fig. 8. The results for the alkali and alkaline earth metal ion forms in comparison with the native form (Na^+) are shown in Fig. 8a and 8b, while those for the transition metal ion forms are presented in Fig. 8c and 8d. The shape of the breakthrough curve mainly depends on the adsorption equilibrium, while the broadness originates from mass (and heat) transfer resistances in the porous materials and fluid mixing [57]. For alkali and alkaline earth metal ions, the broadness of the breakthrough curves is almost identical for each

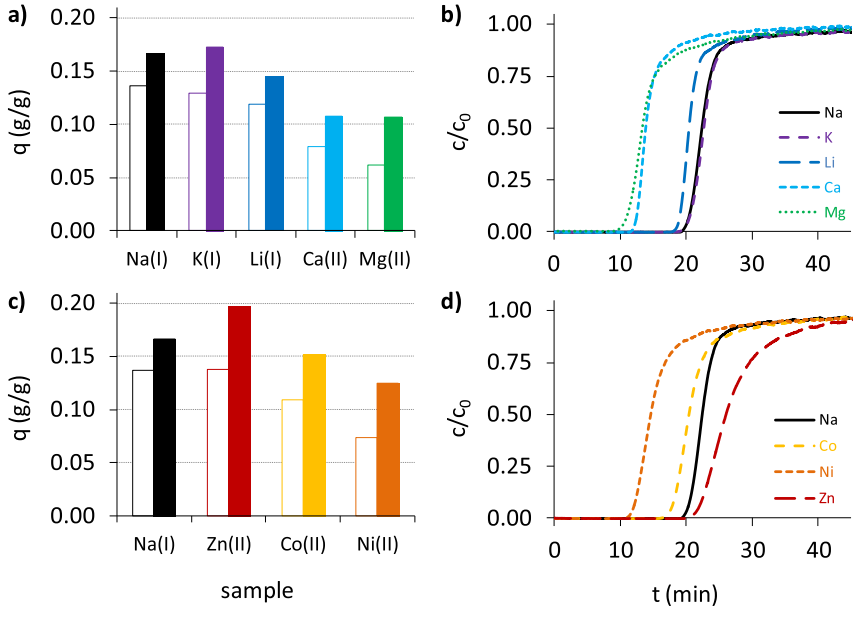

Fig. 8. HCl adsorption capacities (a,c) at saturation (filled) and at 1 ppm (empty), obtained from breakthrough curves (b,d) for alkali and alkaline earth (a,b) and transition metal (c,d) exchanged X zeolite materials. Breakthrough curves were recorded at 298 K, 0.34 m/s gas velocity, 6.39 mbar HCl partial pressure and 30 bar total pressure.

form. This indicates that the mass transfer resistances are not significantly affected by the type of cation present in the zeolite material. Only the Mg^{2+} form exhibits a wider mass transfer zone than the other samples, with the largest observed difference in both adsorption capacities (i.e. at saturation and at 1 ppm) among the different samples shown in Fig. 8b. Thus, the ion-exchange of Na^+ for Mg^{2+} leads to less favorable HCl uptake kinetics, compared to the other ion-exchanges samples, possibly originating from different metal species being taken up from the electrolyte solution or the location of the cation in the zeolite pores [100]. An attempt to connect the observed HCl removal performances with the material properties is discussed further in more detail.

On the other hand, very clear differences are observed in terms of average breakthrough time between the various samples (Fig. 8b). This expresses the differences in amount HCl adsorbed as shown in Fig. 8a. While the native (Na^+) and K^+ forms display almost identical breakthrough curves (Fig. 8b) and, thus, nearly equal adsorption capacities (Fig. 8a), shorter (average) breakthrough times are seen for Li^+, Ca^{2+} and Mg^{2+} forms (Fig. 8b), leading to lower HCl adsorbed amounts (Fig. 8a). The difference is limited for the Li^+ form, but significant for the Mg^{2+} and Ca^{2+} forms. This shows that the Li^+, which resides with Na^+ in material pore environment (see exchange %, Table 2), may result in a less favorable bi-metal system than K^+ for HCl uptake. It is known that a specific cation ratio is required for the enhancement of adsorption separation performance of gasses with Li^+ exchanged zeolite materials [101]. The significant reduction in adsorbed amount for the Mg^{2+} and Ca^{2+} forms, however, the cause remains unclear, possibly originating from the double charge.

For the transition metal ion forms (Fig. 8c,d), different observations can be made compared to the alkali and alkaline earth ion-exchanged samples (Fig. 8a,b). First, all transition metal ion samples possess wider breakthrough profiles than the native material, indicating that the ion-exchange resulted in an increase in mass transfer resistances (Fig. 8d). The different metal species and/or locations in the zeolite pore environment may be at the origin of this result [102]. Second, although ion-exchange of the native cation (Na^+) for Zn^{2+} significantly increases the amount of HCl being adsorbed on the X zeolite material (Fig. 8c), a small and large decrease is observed for the Co^{2+} and Ni^{2+} forms, respectively, compared to the native material. The improvement of the native material with Zn^{2+} may be assigned to the over-exchange (Table 2). The difference between the samples containing the Co^{2+} and Ni^{2+} cations can be attributed to the accessibility of the pores, as seen from the porosities given in Table 2. Interestingly, in general, for double charged cations, the transition metal ion forms perform better than the alkaline earth metal ion samples in terms of adsorption capacities, but lead to broader breakthrough profiles.

In order to further evaluate the HCl removal performances of the different ion-exchanged X zeolite samples, the adsorption capacities given in Fig. 8 were converted from mass HCl adsorbed per mass loaded sample into the amount of HCl molecules adsorbed per cation and per (positive cation) charge (see Supporting Information S10). The results are shown in Fig. 9. First, the materials containing (only) single charged cations, being the alkali metal ion Na^+, K^+ and Li^+ forms, adsorb about one HCl molecule per cation, which is in line with the previous discussion on the nature and mechanism of HCl adsorption (see Section 3.3.2.). Each cation will therefore form a salt molecule M-Cl (with M being the cation atom) in the material pores. For transition metal ions (i.e. Zn^{2+}, Co^{2+}, Ni^{2+}), being double charged, approximatively two HCl molecule are adsorbed per cation atom. This suggests that each double charged cation will react with two HCl molecules into a salt molecule of the type M-Cl_2. Since the ion-exchange is not fully completed (Table 2) about 1.6 HCl adsorb molecules per cation is expected

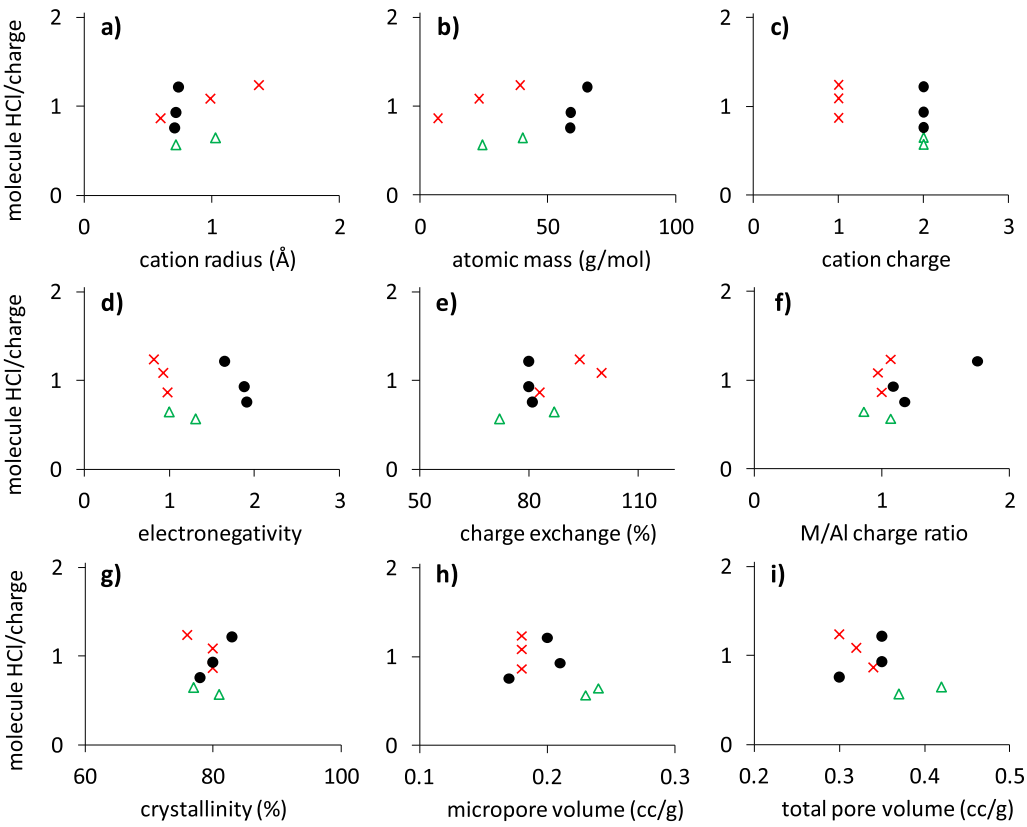

Fig. 10. HCl adsorption capacities in terms of adsorbed molecules HCl per charge as a function of cation properties (Table 2), for (×) alkali, (△) alkaline earth and (●) transition metal ion-exchanged X zeolite materials. The adsorption capacities were calculated following the procedure provided in Supporting Information Section S10.

for the double charged ion-exchanged samples (Fig. 9). While this corresponds quite well with the results for the Co^{2+} and Ni^{2+} forms, the Zn^{2+} form adsorbs significantly more HCl molecules than expected per cation in the zeolite pores. This result is attributed to the Zn^{2+} over-exchange (Table 2), since in the calculation only the cations in the zeolite are counted (see Supporting Information, Section S10). In contrary, double charged alkaline earth metal ion samples only take up about one molecule of HCl per cation. The Mg^{2+} and Ca^{2+} ion-exchanged samples may offer a less favourable environment for HCl adsorption compared to the other materials, however, the origin remains unclear. Since a three atomic salt molecule of the type $M\text{-}Cl_2$ is expected to be formed with double charged cations, the changes to have simultaneously two HCl molecules colliding together with the cation is smaller than a single HCl molecule colliding with a single charged cation. Possibly, the alkaline earth metal ions offer a less stabilizing environment compared to the transition metal ions during the reaction with HCl into a salt molecule. However, the elucidation of this difference lies beyond the scope of this study. Furthermore, the different tendencies observed in amount adsorbed per cation are also clearly depicted in terms of HCl molecules adsorbed per (positive cation) charge (Fig. 9). While alkali and transition metal ions tend to maximize the use of their charges to adsorb one HCl per charge, the alkaline earth metal ions Mg^{2+} and Ca^{2+} shows only about half of the expected (adsorption equilibrium) performance.

An attempt was made to correlate the HCl removal performances of the different samples (see above) in terms of molecules HCl adsorbed per charge with the different cation and material properties given in Table 2. The different comparisons are shown in Fig. 10 per cation group (i.e. alkali, alkaline earth and transition metals). First, the amount of HCl molecules adsorbed per charge increases with cation radius (Fig. 10a) and atomic mass (Fig. 10b) within each cation group. A larger cation may stabilize more efficiently its (pore) environment than a smaller cation upon reaction with HCl [103], resulting in an increased HCl uptake. Different tendencies can be seen in the literature for ion-exchanged zeolite separation and catalytic performances. During (physical) adsorption an increase in saturation capacity is observed with decreasing cation radius [50]. At low loading the opposite trend is typically noticed [104]. For chemical reactions higher conversions are seen with larger cations [105].

Second, no clear preference in (cation) charge is seen in Fig. 10c. A small (average) preference for single charged cations is observed compared to double charged cations, which is mainly attributed to the badly performing double charged alkaline earth metal cations (Fig. 10c). Next, interestingly, within each group a clear tendency is observed between the amounts of HCl molecules adsorbed per (positive cation) charge and the electronegativity (Fig. 10d). The less electronegative the cation, the more HCl molecules are adsorbed on the zeolite material. This can be understood by the acid-base properties of zeolite framework, where the exchangeable cation act as an acid site and the framework oxygen nearest to this site provides a basic site. This basicity increases as the cation electronegativity decreases, leading to high HCl capture [50]. Furthermore, the amount HCl being adsorbed appears to be unaffected by the degree of ion-exchange (Fig. 10e), indicating that all cations present in the material (i.e. native and exchanged) are participating into the HCl uptake. In addition, Fig. 10f shows that the small variations in charge balance does not affect the HCl adsorption. The over-exchange, seen from the large charge ratio, seems to improve, but not significantly, the HCl uptake. Over-exchanged zeolites were seen to improve the catalytic performance of the zeolite materials, such as during the reduction of NO_x [106]. The effect of over-exchange on the HCl removal performance from hydrogen gas by zeolites will be dedicated for another work. Fig. 10g indicates that the variation of the crystallinity is not large enough to observe any difference between the different samples. Finally, the pore volumes (micro- and total), shown in Fig. 10h and 10i, seem not to influence the HCl adsorption. As long as the cations are accessible or in an accessible form, the reaction with HCl will take place. In conclusion, a complex interplay of various parameters is expected to influence the HCl adsorption (equilibrium) capacities of the ion-exchange X zeolite materials, however, some properties appear to play a more important role, such as the cation radius, mass and electronegativity. Although the native (Na^+), K^+ and Zn^{2+} exchanged X zeolite materials were identified as the most promising adsorbents, the further investigation and understanding of the effect of cation and material properties on the HCl adsorption mechanism and removal performance will allow a fine control and optimization of this hydrogen gas purification.

4. Conclusions

In this study, zeolites with both low and high cation content, as well as ion-exchanged materials, were explored for the removal of HCl from hydrogen gas by adsorption. The zeolite screening indicated that the X zeolite material outperforms the other materials due to the presence of accessible cations. The characterization of the ion-exchanged X materials demonstrated that the ion-exchange was successfully achieved with expected tendencies in XRD and ATR-FTIR spectra, as well as porosities. The breakthrough experiments highlighted a significant effect of hydration with (ambient) hydrated samples showing an improved HCl removal performance in comparison dehydrated samples. Dehydrated sample displayed an earlier HCl breakthrough and a much broader (unfavorable) breakthrough profile. The series of characterization supports the hypothesis that HCl is taken up by the material by reaction with the cations present in the zeolite cavities into salt molecules, with the hydration and cation type influencing the HCl removal performance. For instance, while alkali and transition metal ions tend to maximize the use of their charges to adsorb and react with one HCl per charge, the alkaline earth metal ions Mg^{2+} and Ca^{2+} shows only about half of the expected (adsorption equilibrium) performance. Only the Zn^{2+} exchanged X zeolite presented an improvement in the HCl adsorption capacity at saturation in comparison to native (Na^+) X zeolite, which was attributed to the over-exchange of the zeolite cations. The investigation also pinpointed that parameters such as cation mass, radius and electronegativity play an important role in the HCl removal performance. Finally, although the native (Na^+), K^+ and Zn^{2+} exchanged X zeolite materials were identified as the most promising adsorbents, towards the implementation in a separation process the material reusability should be explored.

Acknowledgments

Julien Cousin-Saint-Remi and Joeri Denayer thank the FWO Vlaanderen for the financial support (12P2217N and 1512118N). Graphical abstract was supported by Ch. Baerlocher and L.B. McCusker, Database of Zeolite Structures: http://www.iza-structure.org/databases/.

Appendix A. Supplementary data

Supplementary data to this article can be found online at https://doi.org/10.1016/j.cej.2019.122512.

References

[1] D. Wang, S. Czernik, E. Chornet, Production of hydrogen from biomass by catalytic steam reforming of fast pyrolysis oils, Energy Fuels 12 (1998) 19–24.
[2] M. Momirlan, T.N. Veziroglu, The properties of hydrogen as fuel tomorrow in sustainable energy system for a cleaner planet, Int. J. Hydrogen Energy 30 (2005) 795–802.
[3] C. Acar, I. Dincer, Comparative assessment of hydrogen production methods from renewable and non-renewable sources, Int. J. Hydrogen Energy 39 (2014) 1–12.
[4] R. Ramachandran, R.K. Menon, An overview of industrial uses of hydrogen, Int. J. Hydrogen Energy 23 (1998) 593–598.
[5] L. Barreto, A. Makihira, K. Riahi, The hydrogen economy in the 21st century: A sustainable development scenario, Int. J. Hydrogen Energy 28 (2003) 267–284.

[6] N. Eliaz, D. Eliezer, D.L. Olson, Hydrogen-assisted processing of materials, Mater. Sci. Eng., A 289 (2000) 41–53.
[7] C.J. Winter, Hydrogen as an energy carrier — a guide, Hydrog. Energy Carr. (2012).
[8] P.P. Edwards, V.L. Kuznetsov, W.I.F. David, N.P. Brandon, Hydrogen and fuel cells: Towards a sustainable energy future, Energy Policy. 36 (2008) 4356–4362.
[9] M. Wietschel, M. Ball, The future of hydrogen – opportunities and challenges, Int. J. Hydrogen Econ. 34 (2009) 615–627.
[10] Chien. C. Chao, Process for removing HCl from hydrocarbon streams, U.S. Pat. No. 5,688,479. U.S. Pat. Trademark Off. Washington, D.C., 1997.
[11] Hubert L. Fleming, Kenneth P. Goodboy, Emmanuel K. Saforo, Adsorbent for HCl comprising alumina and acid-treated Y zeolite, U.S. Pat. No. 4,762,537. U.S. Pat. Trademark Off. Washington, D.C., 1994.
[12] John S. Lee, Micehal J. Pearson, HCl adsorbent and method for making and using same, U.S. Pat. No. 5,316,998. U.S. Pat. Trademark Off. Washington, D.C., 1988.
[13] M.T. Lee, Z.Q. Wang, J.R. Chang, Activated-carbon-supported NaOH for removal of HCL from reformer process streams, Ind. Eng. Chem. Res. 42 (2003) 6166–6170.
[14] L. Micoli, G. Bagnasco, M. Turco, HCl removal from biogas for feeding MCFCs: Adsorption on microporous materials, Int. J. Hydrogen Energy 38 (2013) 447–452.
[15] J. K., Industrial Organic Chemistry, Nature, 2008.
[16] W. Balthasar, Hydrogen production and technology: today, tomorrow and beyond, Int. J. Hydrogen Energy 9 (1984) 649–668.
[17] J.Y. Kim, Y.C. Park, S.H. Jo, H.J. Ryu, J.I. Baek, J.H. Moon, The absorption breakthrough characteristics of hydrogen chloride gas mixture on potassium-based solid sorbent at high temperature and high pressure, Energy Fuels 30 (2016) 2268–2275.
[18] G. Mura, A. Lallai, On the kinetics of dry reaction between calcium oxide and gas hydrochloric acid, Chem. Eng. Sci. 47 (1992) 2407–2411.
[19] T. Kameda, N. Uchiyama, T. Yoshioka, Treatment of gaseous hydrogen chloride using Mg-Al layered double hydroxide intercalated with carbonate ion, Chemosphere 81 (2010) 658–662.
[20] T. Kameda, N. Uchiyama, T. Yoshioka, Removal of HCl, SO2, and NO by treatment of acid gas with Mg-Al oxide slurry, Chemosphere 82 (2011) 587–591.
[21] M. Hartman, K. Svoboda, M. Pohořelý, M. Šyc, S. Skoblia, P.C. Chen, Reaction of hydrogen chloride gas with sodium carbonate and its deep removal in a fixed-bed reactor, Ind. Eng. Chem. Res. 53 (2014) 19145–19158.
[22] W. Duo, N.F. Kirkby, J.P.K. Seville, J.H.A. Kiel, A. Bos, H. Den Uil, Kinetics of HCl reactions with calcium and sodium sorbents for IGCC fuel gas cleaning, Chem. Eng. Sci. 51 (1996) 2541–2546.
[23] A.B. de Haan, H. Bosch, Indust. Sep. Process. (2013).
[24] B.L. Dou, J.S. Gao, X.Z. Sha, A study on the reaction kinetics of HCl removal from high-temperature coal gas, Fuel Process. Technol. 72 (2001) 23–33.
[25] B. Dou, B. Chen, J. Gao, X. Sha, Reaction of solid sorbents with hydrogen chloride gas at high temperature in a fixed-bed reactor, Energy Fuels 19 (2005) 2229–2234.
[26] N. Verdone, P. De Filippis, Reaction kinetics of hydrogen chloride with sodium carbonate, Chem. Eng. Sci. 61 (2006) 7487–7496.
[27] B. Dou, W. Pan, J. Ren, B. Chen, J. Hwang, T.U. Yu, Single and combined removal of HCl and alkali metal vapor from high-temperature gas by solid sorbents, Energy Fuels 21 (2007) 1019–1023.
[28] T. Kameda, N. Uchiyama, K.S. Park, G. Grause, T. Yoshioka, Removal of hydrogen chloride from gaseous streams using magnesium-aluminum oxide, Chemosphere 73 (2008) 844–847.
[29] Y. Ohtsuka, N. Tsubouchi, T. Kikuchi, H. Hashimoto, Recent progress in Japan on hot gas cleanup of hydrogen chloride, hydrogen sulfide and ammonia in coal-derived fuel gas, Powder Technol. 190 (2009) 340–347.
[30] M. Sharma, R.K. Vyas, K. Singh, A review on reactive adsorption for potential environmental applications, Adsorption. 19 (2013) 161–188.
[31] F.A. Kloutse, A. Hourri, S. Natarajan, P. Benard, R. Chahine, Hydrogen separation by adsorption: Experiments and modelling of H2-N2-CO2 and H2-CH4-CO2 mixtures adsorption on CuBTC and MOF-5, Microporous Mesoporous Mater. 271 (2018) 175–185.
[32] S. Lin, M. Harada, Y. Suzuki, H. Hatano, Hydrogen production from coal by separating carbon dioxide during gasification, Fuel 81 (2002) 2079–2085.
[33] S. Liang, Z. Fan, W. Zhang, M. Guo, F. Cheng, M. Zhang, Controllable growth of Na2CO3 fibers for mesoporous activated alumina ball modification towards the high-efficiency adsorption of HCl gas at low temperature, RSC Adv. 7 (2017) 53306–53315.
[34] A. Ephraim, L. Ngo, D.P. Minh, D. Lebonnois, C. Peregrina, P. Sharrock, A. Nzihou, Valorization of Waste-Derived Inorganic Sorbents for the Removal of HCl in Syngas, Waste Biomass Valorization (2018) 1–12.
[35] A. Dal Pozzo, R. Moricone, A. Tugnoli, V. Cozzani, Experimental investigation of the reactivity of sodium bicarbonate toward hydrogen chloride and sulfur dioxide at low temperatures, Ind. Eng. Chem. Res. 58 (2019) 6316–6324.
[36] F.V.S. Lopes, C.A. Grande, A.E. Rodrigues, Activated carbon for hydrogen purification by pressure swing adsorption: Multicomponent breakthrough curves and PSA performance, Chem. Eng. Sci. 66 (2011) 303–317.
[37] Z. Wang, H. Liu, K. Zhou, P. Fu, H. Zeng, J. Qiu, Effect of surface oxygen/nitrogen groups on hydrogen chloride removal using modified viscosebased activated carbon fibers, RSC Adv. 5 (2015) 86006–86012.
[38] W. Sievers, A. Mersmann, Single and multicomponent adsorption equilibria of carbon dioxide, nitrogen, carbon monoxide and methane in hydrogen purification processes, Chem. Eng. Technol. 17 (1994) 325–337.
[39] S. Sircar, T.C. Golden, Purification of hydrogen by pressure swing adsorption, Sep. Sci. Technol. 35 (2000) 667–687.
[40] J. Dong, Y.S. Lin, W. Liu, Multicomponent hydrogen/hydrocarbon separation by MFI-type zeolite membranes, AIChE J. 46 (2000) 1957–1966.
[41] M.W. Ackley, S.U. Rege, H. Saxena, Application of natural zeolites in the purification and separation of gases, Microporous Mesoporous Mater. 61 (2003) 25–42.
[42] S. Kulprathipanja, Zeolites in Industrial Separation and Catalysis, 2010.
[43] J.Y. Kim, D.H. Kyung, Y.C. Park, S.H. Jo, H.J. Ryu, Y.S. Park, J.H. Moon, The adsorption and desorption breakthrough behavior of hydrogen chloride gas mixture on zeolite 13X pellet in a fixed bed reactor, J. Chem. Eng. Japan 48 (2015) 202–211.
[44] R.M. Barrer, Ion-exchange and ion-sieve processes in crystalline zeolites, J. Chem. Soc. (1950) 2342–2350.
[45] W.J. Mortier, Zeolite electronegativity related to physicochemical properties, J. Catal. 55 (1978) 138–145.
[46] P.A. Jacobs, M. Tielen, J.B. Uytterhoeven, Active sites in zeolites. Part 6. Alcohol dehydration over alkali cation-exchanged X and Y zeolites, J. Catal. 50 (1977) 98–108.
[47] M.W. Ackley, R.T. Yang, Diffusion in ion-exchanged clinoptilolites, AIChE J. 37 (1991) 1645–1656.
[48] M.S.A. Baksh, E.S. Kikkinides, R.T. Yang, Lithium type X zeolite as a superior sorbent for air separation, Sep. Sci. Technol. 27 (1992) 277–294.
[49] S.T. Yang, J. Kim, W.S. Ahn, CO2 adsorption over ion-exchanged zeolite beta with alkali and alkaline earth metal ions, Microporous Mesoporous Mater. 135 (2010) 90–94.
[50] K.S. Walton, M.B. Abney, M.D. LeVan, CO2 adsorption in y and X zeolites modified by alkali metal cation exchange, Microporous Mesoporous Mater. 91 (2006) 78–84.
[51] K. Kusakabe, T. Kuroda, S. Morooka, Separation of carbon dioxide from nitrogen using ion-exchanged faujasite-type zeolite membranes formed on porous support tubes, J. Memb. Sci. 148 (1998) 13–23.
[52] D. Bonenfant, M. Kharoune, P. Niquette, M. Mimeault, R. Hausler, Advances in principal factors influencing carbon dioxide adsorption on zeolites, Sci. Technol. Adv. Mater. 9 (2008) 013007.
[53] L. Ćurković, Š. Cerjan-Stefanović, T. Filipan, Metal ion exchange by natural and modified zeolites, Water Res. 31 (1997) 1379–1382.
[54] H. Yahiro, M. Iwamoto, Copper ion-exchanged zeolite catalysts in deNOxreaction, Appl. Catal. A Gen. 222 (2001) 163–181.
[55] J. Landers, G.Y. Gor, A.V. Neimark, Density functional theory methods for characterization of porous materials, Colloids Surfaces A Physicochem. Eng. Asp. 437 (2013) 3–32.
[56] M. Thommes, K.A. Cychosz, Physical adsorption characterization of nanoporous materials: Progress and challenges, Adsorption. 20 (2014) 233–250.
[57] D.M. Ruthven, Principles of adsorption and adsorption processes, Chem. Eng. Process Process. Intensif. (1985).
[58] K. Kotoh, K. Kimura, Y. Nakamura, K. Kudo, Hydrogen isotope separation using molecular sieve of synthetic zeolite 3A, Fusion Sci. Technol. 54 (2008) 419–422.
[59] D.W. Breck, W.G. Eversole, R.M. Milton, T.B. Reed, T.L. Thomas, Crystalline zeolites. I. The Properties of a new synthetic zeolite, type A, J. Am. Chem. Soc. 78 (1956) 5963–5972.
[60] C.A. Grande, C. Gigola, A.E. Rodrigues, Adsorption of propane and propylene in pellets and crystals of 5A zeolite, Ind. Eng. Chem. Res. 41 (2002) 85–92.
[61] Database of Zeolites Structures. http://www.iza-structure.org. Accessed 09 January 2019.
[62] G. Zaikov, The concept of micellar-sponge nanophases in chemical, Phys. Polym. (2012).
[63] E.M. Flanigen, J.M. Bennett, R.W. Grose, J.P. Cohen, R.L. Patton, R.M. Kirchner, J.V. Smith, Silicalite, a new hydrophobic crystalline silica molecular sieve, Nature 271 (1978) 512.
[64] G. Busca, Acidity and basicity of zeolites: A fundamental approach, Microporous Mesoporous Mater. 254 (2017) 3–16.
[65] M. Jeffroy, A. Boutin, A.H. Fuchs, Understanding the equilibrium ion exchange properties in faujasite zeolite from monte carlo simulations, J. Phys. Chem. B 115 (2011) 15059–15066.
[66] A. Maes, A. Cremers, Ion exchange of synthetic zeolite X and Y with Co2+, Ni2+, Cu2+and Zn2+ions, J. Chem. Soc. Faraday Trans. 1 Phys. Chem. Condens. Phases. 71 (1975) 265–277.
[67] K.R. Franklin, R.P. Townsend, Multicomponent ion exchange in zeolites. Part 4. – The exchange of magnesium ions in zeolites X and Y, J. Chem. Soc. Faraday Trans. 1 Phys. Chem. Condens. Phases 84 (1988) 2755–2770.
[68] D. Bae, S. Zhen, K. Seff, Structure of dehydrated Zn 2+ -exchanged zeolite X. Overexchange, framework dealumination and reorganization, stoichiometric retention of monomeric tetrahedral aluminate, J. Phys. Chem. B 103 (1999) 5631–5636.
[69] E.S. Shpiro, W. Grünert, R.W. Joyner, G.N. Baeva, Nature, distribution and reactivity of copper species in over-exchanged Cu-ZSM-5 catalysts: an XPS/XAES study, Catal. Letters. 24 (1994) 159–169.
[70] Y. Marcus, Ionic radii in aqueous solutions, J. Solution Chem. 88 (1983) 1475–1498.
[71] A.G. Gaydon, Handbook of Chemistry and Physics, 47th ed., Phys, Bull, 2015.
[72] M.M.J. Treacy, J.B. Higgins, Collection of Simulated XRD Powder Patterns for Zeolites Fifth (5th) Revised Edition, 2007. doi:10.1016/B978-0-444-53067-7.X5470-7.
[73] F. Chung, D. Smith, Industrial Applications of X-Ray Diffraction, 2014.
[74] T.M. Nenoff, J.B. Parise, G.A. Jones, L.G. Galya, D.R. Corbin, G.D. Stucky, Flexibility of the zeolite RHO framework. In situ X-ray and neutron powder structural characterization of cation-exchanged BePO and BeAsO RHO analogs†, J. Phys. Chem. 100 (1996) 14256–14264.

[75] A. Ertan, F. Çakicioğlu-Özkan, CO2 and N2 adsorption on the acid (HCl, HNO 3, H2SO4 and H3PO4) treated zeolites, Adsorption 11 (2005) 151–156.
[76] B.A. Holmberg, H. Wang, Y. Yan, High silica zeolite Y nanocrystals by dealumination and direct synthesis, Microporous Mesoporous Mater. 74 (2004) 189–198.
[77] W. Mozgawa, M. Król, K. Barczyk, FT-IR studies of zeolites from different structural groups, Chemik 65 (2011) 667–674.
[78] W.P.J.H. Jacobs, J.H.M.C. van Wolput, R.A. van Santen, An in situ Fourier transform infrared studyof zeolitic vibrations: Dehydration, deammoniation, and reammoniation of ion-exchanged Y zeolites, Zeolites 13 (1993) 170–182.
[79] J.-H. Moon, S.-J. Lee, D.-K. Choi, Y.-J. Park, C.-H. Lee, Adsorption equilibria of O 2, N 2, and Ar on carbon molecular sieve and zeolites 10X, 13X, and LiX, J. Chem. Eng. Data 51 (2006) 1001–1008.
[80] M.J. Carmo, J.C. Gubulin, Ethanol-water adsorption on commercial 3A zeolites: kinetic and thermodynamic data, Brazilian J. Chem. Eng. 14 (1997).
[81] F. Akhtar, L. Andersson, S. Ogunwumi, N. Hedin, L. Bergström, Structuring adsorbents and catalysts by processing of porous powders, J. Eur. Ceram. Soc. 34 (2014) 1643–1666.
[82] J. Wang, F. Xu, W. Jie Xie, Z. Jian Mei, Q. Zhuo Zhang, J. Cai, W. Min Cai, The enhanced adsorption of dibenzothiophene onto cerium/nickel-exchanged zeolite Y, J. Hazard. Mater. 163 (2009) 538–543.
[83] M.L.M. Oliveira, A.A.L. Miranda, C.M.B.M. Barbosa, C.L. Cavalcante, D.C.S. Azevedo, E. Rodriguez-Castellon, Adsorption of thiophene and toluene on NaY zeolites exchanged with Ag(I), Ni(II) and Zn(II), Fuel 88 (2009) 1885–1892.
[84] M.H. Simonot-Grange, A. Elm'Chaouri, G. Weber, P. Dufresne, F. Raatz, J.F. Joly, Characterization of the dealumination effect into H faujasites by adsorption: Part 1. The water molecule as a structural aluminum ion selective probe, Zeolites 12 (1992) 155–159.
[85] V.K. Chuikina, A.V. Kiselev, L.V. Mineyeva, G.G. Muttik, Heats of adsorption of water vapour on NaX and KNaX zeolites at different temperatures, J. Chem. Soc. Faraday Trans. 1 Phys. Chem. Condens. Phases 72 (1976) 1345-1354.
[86] O.M. Dzhigit, A.V. Kiselev, K.N. Mikos, G.G. Muttik, T.A. Rahmanova, Heats of adsorption of water vapour on X-zeolites containing Li +, Na +, K +, Rb +, and Cs + cations, Trans. Faraday Soc. 67 (1971) 458–467.
[87] V. Middelkoop, K. Coenen, J. Schalck, M. Van, Sint Annaland, F. Gallucci, 3D printed versus spherical adsorbents for gas sweetening, Chem. Eng. J. 357 (2019) 309–319.
[88] V. Garshasbi, M. Jahangiri, M. Anbia, Equilibrium CO2adsorption on zeolite 13X prepared from natural clays, Appl. Surf. Sci. 393 (2017) 225–233.
[89] I.J. Gal, P. Radovanov, Ion-exchange equilibria of synthetic 13X zeolite with Ni2 +, Co2 +, Zn2 + and Cd2 + ions, J. Chem. Soc. Faraday Trans. 1 Phys. Chem. Condens. Phases 71 (1975) 1671–1677.
[90] L. Zhu, K. Seff, Reinvestigation of the crystal structure of dehydrated sodium zeolite X, J. Phys. Chem. B 103 (1999) 9512–9518.
[91] Y.H. Yeom, S.B. Jang, Y. Kim, S.H. Song, K. Seff, Three crystal structures of vacuum-dehydrated zeolite X, M46Si100Al92O384, M = Mg2 +, Ca2 +, and Ba2 +, J. Phys. Chem. B 101 (1997) 6914–6920.
[92] M. Fan, H. Panezai, J. Sun, S. Bai, X. Wu, Thermal and kinetic performance of water desorption for N2 adsorption in Li-LSX zeolite, J. Phys. Chem. C 118 (2014) 23761–23767.
[93] J.A. Delgado, V.I. Águeda, M.A. Uguina, J.L. Sotelo, P. Brea, C.A. Grande, Adsorption and diffusion of H2, CO, CH4, and CO2 in BPL activated carbon and 13X zeolite: Evaluation of performance in pressure swing adsorption hydrogen purification by simulation, Ind. Eng. Chem. Res. 53 (2014) 15414–15426.
[94] R. Schöllner, W.D. Einicke, B. Gläser, Liquid-phase adsorption of monosaccharide-water mixtures on X and Y zeolites, J. Chem. Soc., Faraday Trans. 89 (1993) 1871–1876.
[95] Z. Song, G. Liu, D. He, X. Pang, Y. Tong, Y. Wu, D. Yuan, Z. Liu, Y. Xu, Acetylene hydrochlorination over 13X zeolite catalysts at high temperature, Green Chem. 18 (2016) 5994–5998.
[96] M. Lee, X-Ray Diffraction for Materials Research, 2016. doi:10.1201/b19936.
[97] J. Weitkamp, Zeolites and catalysis, Solid State Ionics 131 (2000) 175–188.
[98] H. Esemann, H. Förster, E. Geidel, K. Krause, Exploring cation siting in zeolite ZSM-5 by infrared spectroscopy, EXAFS and computer simulations, Micropor. Mater. 6 (1996) 321–329.
[99] F.T. Wagner, T.E. Moylan, Hydrogen chloride adsorption and coadsorption with hydrogen or water on platinum (111), Surf. Sci. 216 (1989) 361–385.
[100] G. Sethia, R.S. Somani, H. Chand Bajaj, Adsorption of carbon monoxide, methane and nitrogen on alkaline earth metal ion exchanged zeolite-X: Structure, cation position and adsorption relationship, RSC Adv. 5 (2015) 12773–12781.
[101] M.L. Zanota, N. Heymans, F. Gilles, B.L. Su, G. De Weireld, Thermodynamic study of LiNaKLSX zeolites with different Li exchange rate for N2/O2 separation process, Microporous Mesoporous Mater. 143 (2011) 302–310.
[102] E. Ivanova, B. Koumanova, Adsorption of sulfur dioxide on natural clinoptilolite chemically modified with salt solutions, J. Hazard. Mater. 167 (2009) 306–312.
[103] O. Talu, S.Y. Zhang, D.T. Hayhurst, Effect of cations on methane adsorption by NaY, MgY, CaY, SrY, and BaY zeolites, J. Phys. Chem. 97 (1993) 12894–12898.
[104] O. Cheung, N. Hedin, Zeolites and related sorbents with narrow pores for CO2 separation from flue gas, RSC Adv. 4 (2014) 14480–14494.
[105] J. Sebastian, K.M. Jinka, R.V. Jasra, Effect of alkali and alkaline earth metal ions on the catalytic epoxidation of styrene with molecular oxygen using cobalt(II)-exchanged zeolite X, J. Catal. 244 (2006) 208–218.
[106] H.Y. Chen, E.M. El-Malki, X. Wang, R.A. Van Santen, W.M.H. Sachtler, Identification of active sites and adsorption complexes in Fe/MFI catalysts for NO (x) reduction, J. Mol. Catal. A: Chem. 162 (2000) 159–174.